DTU Library

Transverse-mode-selectable microlens vertical-cavity surface-emitting laser

Chung, Il-Sug; Debernardi, Pierluigi; Lee, Yong Tak; Mørk, Jesper

Link back to DTU Orbit

Transverse-mode-selectable microlens vertical-cavity surface-emitting laser

Il-Sug Chung,[1,*] Pierluigi Debernardi,[2] Yong Tak Lee,[3] and Jesper Mørk[1]

[1]DTU Fotonik, Department of Photonics Engineering, Build. 343, Technical University of Denmark, DK-2800 Kgs. Lyngby, Denmark
[2]Istituto di Elettronica e di Ingegneria dell'Informazione e delle Telecomunicazioni, Cosiglio Nazionale Ricerche, Politecnico di Torino, Torino 10129, Italy
[3]Department of Information and Communications, Gwangju Institute of Science and Technology, Gwangju 500-712, Republic of Korea
*ilch@fotonik.dtu.dk

Abstract: A new vertical-cavity surface-emitting laser structure employing a thin microlens is suggested and numerically investigated. The laser can be made to emit in either a high-power Gaussian-shaped single-fundamental mode or a high-power doughnut-shaped higher-order mode. The physical origin of the mode selection properties of the new structure is rigorously analyzed and compared to other structures reported in the literature. The possibility of engineering the emission shape while retaining strong single mode operation is highly desirable for low-cost mid-range optical interconnects applications as well as the compact optical trapping of high-refractive-index dielectric particles and low-refractive-index, absorbing, or metallic particles.

References and links

1. A. Syrbu, A. Mereuta, V. Iakovlev, A. Caliman, P. Royo, and E. Kapon, "10 Gbps VCSELs with high single mode output in 1310 nm and 1550 nm wavelength bands," in *Optical Fiber Communication Conference* (Optical Society of America, 2008), paper OThS2.
2. S.-H. Park, Y. Park, H. Kim, H. Jeon, S. M. Hwang, J. W. Lee, S. H. Nam, B. C. Koh, J. Y. Sohn, and D. S. Kim, "Microlensed vertical-cavity surface-emitting laser for stable single fundamental mode operation," Appl. Phys. Lett. **80**(2), 183–185 (2002).
3. D. Zhou, and L. J. Mawst, "High-power single-mode antiresonant reflecting optical waveguide-type vertical-cavity surface-emitting lasers," IEEE J. Quantum Electron. **38**(12), 1599–1606 (2002).
4. Å. Haglund, J. S. Gustavsson, J. Vukušić, P. Modh, and A. Larsson, "Single fundamental-mode output power exceeding 6 mW from VCSELs with a shallow surface relief," IEEE Photon. Technol. Lett. **16**(2), 368–370 (2004).
5. A. Furukawa, S. Sasaki, M. Hoshi, A. Matsuzono, K. Moritoh, and T. Baba, "High-power single-mode vertical-cavity surface-emitting lasers with triangular holey structure," Appl. Phys. Lett. **85**(22), 5161–5163 (2004).
6. A. Kroner, I. Kardosh, F. Rinaldi, and R. Michalzik, "Towards VCSEL-based integrated optical traps for biomedical applications," Electron. Lett. **42**(2), 93 (2006).
7. A. Ashkin, J. M. Dziedzic, J. E. Bjorkholm, and S. Chu, "Observation of a single-beam gradient force optical trap for dielectric particles," Opt. Lett. **11**(5), 288–290 (1986).
8. K. T. Gahagan, and G. A. Swartzlander, Jr., "Optical vortex trapping of particles," Opt. Lett. **21**(11), 827–829 (1996).
9. A. Kroner, J. F. May, I. Kardosh, F. Rinaldi, H. Roscher, and R. Michalzik, "Novel concepts of vertical-cavity laser-based optical traps for biomedical applications," Proc. SPIE **6191**, 619112 (2006).
10. K. Sakai, and S. Noda, "Optical trapping of metal particles in doughnut-shaped beam emitted by photonic-crystal laser," Electron. Lett. **43**(2), 107 (2007).
11. D. Ohnishi, T. Okano, M. Imada, and S. Noda, "Room temperature continuous wave operation of a surface-emitting two-dimensional photonic crystal diode laser," Opt. Express **12**(8), 1562–1568 (2004).
12. G. P. Bava, P. Debernardi, and L. Fratta, "Three-dimensional model for vectorial fields in vertical-cavity surface-emitting lasers," Phys. Rev. A **63**(2), 023816 (2001).
13. P. Bienstman, R. Baets, J. Vukusic, A. Larsson, M. J. Noble, M. Brunner, K. Gulden, P. Debernardi, L. Fratta, G. P. Bava, H. Wenzel, B. Klein, O. Conradi, R. Pregla, S. A. Riyopoulos, J.-F. P. Seurin, S. L. Chuang, "Comparison of optical VCSEL models on the simulation of oxide-confined devices," IEEE J. Quantum Electron. **37**(12), 1618–1631 (2001).

14. P. Debernardi, J. M. Ostermann, M. Feneberg, C. Jalics, and R. Michalzik, "Reliable polarization control of VCSELs through monolithically integrated surface gratings: a comparative theoretical and experimental study," IEEE J. Selected Topics in Quant. Electron. **11**(1), 1–10 (2005).
15. P. Debernardi, B. Kögel, K. Zogal, P. Meissner, M. Maute, M. Ortsiefer, G. Böhm, and M.-C. Amann, "Modal properties of long-wavelength tunable MEMS-VCSELs with curved mirrors: Comparison of experiment and modeling," IEEE J. Quantum Electron. **44**(4), 391–399 (2008).
16. P. Debernardi, A. Kroner, F. Rinaldi, and R. Michalzik, "Surface relief versus standard VCSELs: a comparison between experimental and hot-cavity model results," IEEE J. Sel. Top. Quantum Electron. **15**(3), 828–837 (2009).
17. A. W. Snyder, and J. D. Love, *Optical waveguide theory*, (Chapman & Hall, 1983).

1. Introduction

A new vertical-cavity surface-emitting laser (VCSEL) structure incorporating a monolithically integrated microlens, hereafter called microlens VCSEL, is suggested. This structure can exhibit high-power emission into either a focused (Gaussian-shaped) single-mode beam profile or a doughnut-shaped beam profile, which have important applications in local area/metropolitan optical fiber networks and compact optical tweezers. The new structure is identified on the basis of a new method for analyzing the mode-selection properties, which is applied to a number of different structures suggested in the literature. This leads to new insight into the mode selection properties governing VCSELs with structured mirrors.

The single-mode high-power microlens VCSEL may be an attractive source for optical interconnects with transmission distances in the order of 10–100 km [1], where the single-mode distributed feedback (DFB) laser is currently the solution. Firstly, single-mode high-power VCSELs consume 5 to 10 times less power than typical DFBs; small power consumption of a laser and its driver can be an important advantage for high-speed multi-channel arrays. Secondly, an integrated microlens can considerably reduce the packaging cost compared to an expensive aspheric lens for DFB lasers, which is needed to improve the efficiency of coupling to single-mode optical fibers. The first investigation of microlens structures incorporated into a VCSEL, demonstrated the possibility of turning a VCSEL, which was originally multimoded, into a single-mode laser by tailoring the lens properties [2]. However, the demonstrated 3-mW single mode output power is considerably smaller than the power levels of 6–7 mW reported for other types of single mode VCSELs; e.g., an anti-resonant VCSEL [3], a surface relief VCSEL [4], and a VCSEL with triangular holey structures [5].

In optical trapping applications, microlens VCSEL based optical tweezers can be attractive for compact biomedical applications and two-dimensional (2D) tweezers arrays, replacing bulky laser and objective lens setups [6]. Two challenges are to obtain Gaussian-shaped high-power emission for the trapping of non-absorbing high-refractive-index particles [7], and to achieve doughnut-shaped high-power emission for the trapping of absorbing, low-refractive-index, or metallic particles [8]. The first approach for the Gaussian-shaped emission, based on a polymer microlens and a surface relief VCSEL, improves the lateral trapping efficiency, but significantly degrades the side mode suppression ratio (SMSR) of higher order modes and the differential quantum efficiency [9]. Regarding the doughnut-shaped output, the first compact approach using a photonic crystal surface emitting laser [10], demonstrates a good lateral trapping force, but its high threshold current of 65 mA and relatively low output power of 4 mW at 95-mA bias current need to be improved [11].

The objectives of this paper are to clearly understand the mode selection mechanism in microlens VCSEL structures, and based on this to suggest new structures that overcome the aforementioned performance limitations of other approaches reported in the literature. As introduced in Section 2, a three-dimensional (3D) vectorial VCSEL simulator was used to precisely deal with the refraction and reflection due to the curved lens surface and the non-concentric geometry of the misaligned microlens with respect to an oxide aperture. In Section 3, the extensive analysis of the first single-mode microlens VCSEL structure [2] reveals that the mode selection does not rely on the effect of focused feedback, as believed so far, but rather on a spatial filtering effect. This new understanding paves the way for novel designs

where either Gaussian- or doughnut-shaped emission can be obtained by appropriately choosing the lens thickness and the radius of curvature. It is also found that the misalignment of a microlens considerably weakens the strength of mode selection. This, we believe, explains the small single-mode output power that was experimentally observed for the first single-mode microlens VCSEL structure [2]. In Section 4, based on this understanding, a new structure employing a thin microlens and doubled topmost DBR layer is suggested, which not only removes the misalignment effect but also provides mode selection strength comparable to surface relief VCSELs. The mode selection strength of the new structure is compared to the surface relief VCSEL (as a reference single mode device), the polymer-microlens surface-relief VCSEL (as a reference optical tweezers device with Gaussian emission), and a plain VCSEL without any structuring (as a reference multi mode device).

2. Device structure and simulation method

In Fig. 1, the five investigated structures are illustrated: (a) A thick microlens VCSEL (the first single-mode microlens VCSEL reported in [2]), two thin microlens VCSELs for (b) Gaussian-shaped and (c) doughnut-shaped outputs (the new structures suggested in this paper), (d) a surface relief VCSEL, and (e) a polymer-microlens surface-relief VCSEL [9]. For comparison we also analyze a simple reference multimode VCSEL, Fig. 1(f), without any structuring of the top surface. The common structure consists of a 24-pair $Al_{0.2}Ga_{0.8}As/Al_{0.92}Ga_{0.08}As$ top DBR, a 1λ-cavity active region, and a 40.5-pair bottom DBR. The 1λ cavity consists of three 7-nm-thick GaAs quantum wells (QWs), 10-nm-thick $Al_{0.3}Ga_{0.7}As$ barrier layers, and 103.8-nm-thick $Al_{0.3}Ga_{0.7}As$ cladding layers. A 20-nm-thick and 15-µm-diameter oxide aperture is situated at the local intensity maximum. The polymer-microlens surface-relief VCSEL has 8-µm-diameter oxide aperture as it does in [9]. The emission wavelength is around 850 nm.
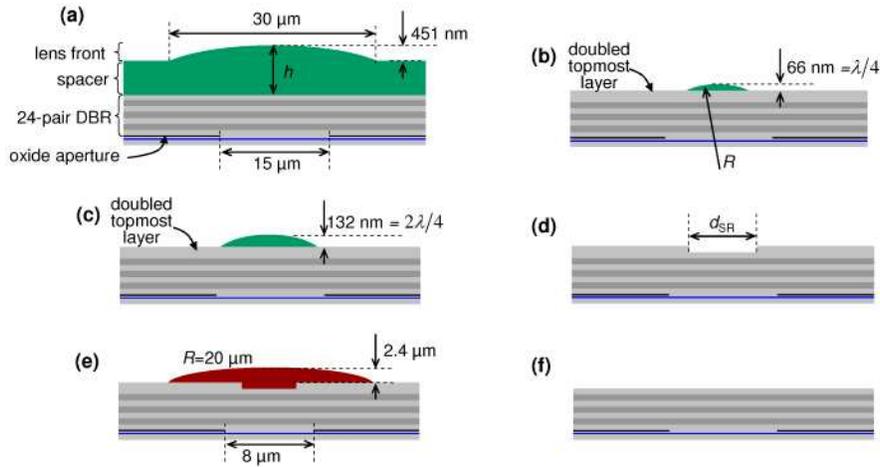

Fig. 1. Schematic profiles of (a) a thick microlens VCSEL [2], (b) a thin microlens VCSEL for Gaussian-shaped emission, (c) a thin microlens VCSEL for doughnut-shaped emission, (d) a surface relief VCSEL, (e) a surface relief VCSEL with a polymer microlens [9], and (f) a reference multimode VCSEL.

For the numerical investigations, a three-dimensional vectorial optical VCSEL simulator based on modal expansion and coupled mode theory [12] was used. In this vectorial approach, the electromagnetic (EM) field distribution is expressed in a basis of Bessel functions. Solving an eigenvalue problem provides both the threshold gain and the expansion coefficients of the EM field distribution of a mode. In this way, refraction and reflection at the microlens interface can be precisely dealt with. Thanks to the modal expansion, the component of the Poynting vector in the growth- (z-) direction can be evaluated. We denotes this the upward Poynting vector, and the analysis of the profile of this vector component turns

out to be a very useful technique for understanding and improving the mode selection properties, as explained in Section 3.

In all simulations, cold cavity conditions are assumed since they suffice for understanding the mode selection mechanism of optical origin. In real devices, single mode operation anticipated by cold cavity simulations can be considerably influenced by effects of thermal lensing or reduced gain-mode overlap. Thus, we require the mode stability factor, S defined in Eq. (1) to exceed 50%. From our experience on single mode VCSEL simulations, single mode operation is maintained over the entire operating range when the S factor exceeds 50%. Following the approaches in [13], a flat optical gain profile in the QW gain region inside the oxide aperture diameter and an imaginary refractive index of 0.01 in the QW absorbing region outside the oxide aperture diameter are assumed.

The reliability of this approach has been verified in the analysis of various VCSEL structures, showing good agreement with experimental results. The investigated structures include a polarization-controlled surface-grating VCSEL [14], a MEMS-tunable VCSEL with a curved mirror [15], and a surface relief VCSEL [16]. Extensive benchmarking comparison with other simulation methods such as the method of lines, Green's function model, eigenmode expansion with PML, etc., [13] also shows excellent agreement.

3. Mode selection mechanism

In order to understand the mechanisms of mode selection we first discuss simulation results for a thick microlens VCSEL. The threshold (material) gain of the 9 lowest modes was calculated as the lens thickness, h, defined in Fig. 1(a), was varied from $44\lambda/4$ (=2906 nm) to $48\lambda/4$ (=3171 nm) by increasing the spacer thickness while keeping the lens front thickness to a constant value of 451 nm. In this paper, λ denotes the effective wavelength inside the material. The radius of curvature (RoC) of the microlens is 250 µm. Figure 2 shows the simulation results as well as the intensity profiles of the investigated modes. The modes are denoted following the nomenclature used in fiber optics [17].
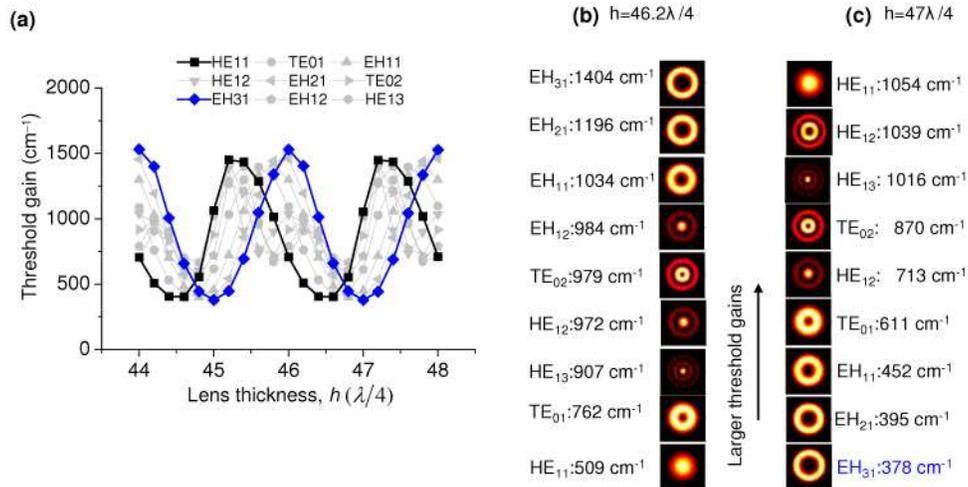

Fig. 2. (a) Threshold gains of the 9 lowest modes vs. lens thickness, h. List of threshold gains with mode intensity profiles for (b) h=46.2λ/4 and (c) h=47λ/4.

The Gaussian- or doughnut-shaped emission can be obtained by appropriately choosing the lens thickness. As shown in Fig. 2(a), when the lens thickness, h equals $46.2\lambda/4$, the fundamental mode, HE_{11} has the smallest threshold gain than other higher modes; the Gaussian-shaped HE_{11} is the only lasing mode at this lens thickness, as shown in Fig. 2(b). With a lens thickness of $47\lambda/4$, the doughnut-shaped mode, EH_{31} with the smallest threshold gain as shown in Figs. 2(a) and 2(c) will lase. The other doughnut-shaped modes, EH_{21} and EH_{11} cannot easily reach lasing conditions: Since the mode profile of EH_{31} is similar to those

of the other doughnut-shaped modes, the gain of these modes will be depleted once the EH_{31} is lasing. However, even in the case of achieving laser operation in one of the other doughnut-shaped modes, the overall emission will be doughnut shaped, which is the key for optical trapping applications.

In Fig. 2(a), the threshold gain of all modes periodically changes as a function of the lens thickness. This periodic behavior results from the interferences occurring near the microlens. A close look at the modal Poynting vector profile supports this explanation. Figure 3 shows a contour plot of the upward Poynting vector of the fundamental mode, HE_{11} and the higher order mode, EH_{31} at $h=46.2\lambda/4$ and $47\lambda/4$. The '+' and '−' signs designate regions of constructive and destructive interferences, respectively: In the '+' region as shown in Fig. 3(a), the reflection from the air-lens interface is, in average, in phase with the other reflections within the top DBR. On the contrary, in the '−' region, it is out of phase, reducing the local reflectivity in that region. The concentric vertical border lines between the '+' and '−' regions are drawn where the local lens thickness equals $(2m\pm0.5)$ $\lambda/4$, with m being an integer number. When $h=46.2$ $\lambda/4$, the interference regions are distributed as shown in Fig. 3(b1/2). The mode HE_{11} has its upward energy flow localized mainly in the central '+' region, as shown in Fig. 3(b1). Thus, a small fraction of the upward energy flow is emitted into the air, which leads to a high modal reflectivity and a small threshold gain. On the contrary, in Fig. 3(b2), a considerable upward energy flow of the mode EH_{31} overlaps with the '−' region and is easily emitted. As a result, the modal reflectivity of the mode EH_{31} becomes smaller than that of HE_{11}, which explains why the mode HE_{11} has a smaller threshold gain than EH_{31} at $h=46.2\lambda/4$ in Fig. 2(a). For $h=47\lambda/4$, the central part now becomes a region of destructive interference, '−' region, as shown in Fig. 3(c1/2). Thus, the mode EH_{31} has a smaller threshold gain than the mode HE_{11}. Since the interference region distribution is purely determined by the lens thickness and RoC, it repeats itself with an increase of the lens thickness by $2\lambda/4$. This explains the periodic behavior of threshold gain as a function of lens thickness in Fig. 2(a), where the observed periodicity is also $2\lambda/4$.
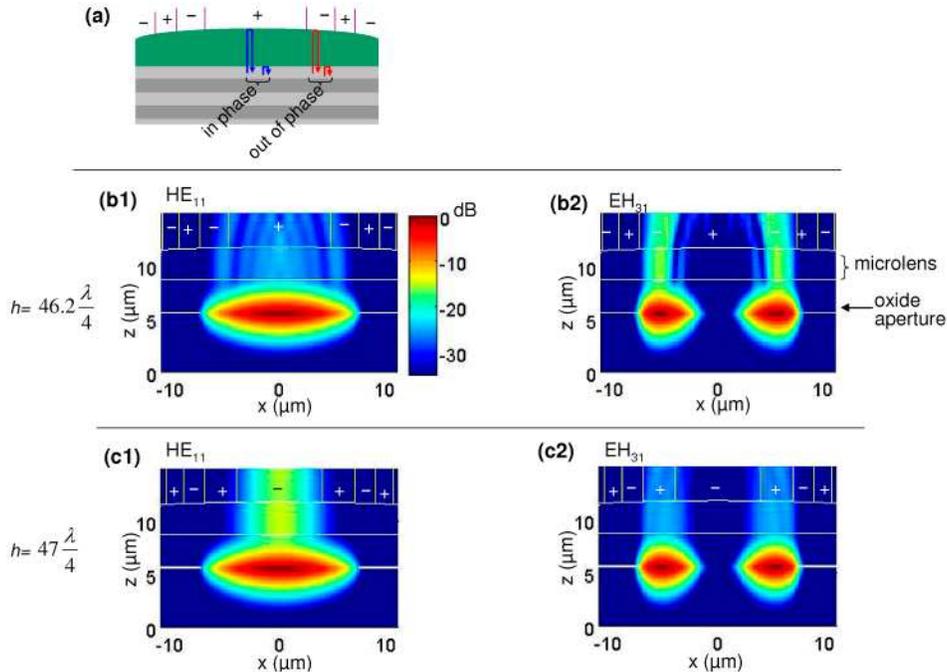

Fig. 3. (a) Illustration of constructive and destructive interferences along the curved lens surface. (b1, b2, c1, c2) Upward Poynting vector profiles. Two modes (HE_{11} and EH_{31}) with two lens thicknesses ($46.2\lambda/4$ and $47\lambda/4$), are compared.

So far, it was believed that focused feedback was the effect leading to the dominance of the fundamental mode in microlens VCSELs [2]. In the focused feedback model, as illustrated in Fig. 4(a), the field, once reflected from the air-lens interface, is multi-reflected between two effective mirror planes: When the multi-reflected beam path is unfolded, the beam propagation is described by Gaussian beam propagation theory, as shown in Figs. 4(b) and 4(c). Since the profile of the fed back beam has a better overlap with the original fundamental mode than with the higher order modes, the fundamental mode can attain a smaller threshold gain. This model suggests a mechanism for the dominance of the fundamental mode, but does not explain the suppression that was observed near $47\lambda/4$ in Fig. 2(a). Furthermore, the periodic behavior observed in Fig. 2(a) cannot be explained: According to the focused feedback model, a small increase of the lens thickness increases the beam path length in Figs. 4(b) and 4(c), leading to a reduction of the transverse size of the feedback at the QW layers. In the focused feedback model it is assumed that the overlap of the fed back beam profile with the original mode profile at the QW layers determines the dominance of a mode [2], and that this is quantitatively reflected in the threshold gain in this paper. Thus, the threshold gain should monotonically change with a monotonic change of the transverse size of the feedback at QW layers, i.e., a monotonic change of the microlens thickness. However, this does not agree with the periodic behaviour obtained by the vectorial simulations. This discrepancy can be attributed to the fact that the interference between the reflection from the air-lens interface and that from the lens-DBR interface is not included in the focused feedback model: It is assumed that multiple reflections occur only between two effective mirror planes once the beam is reflected from the air-lens interface. In addition, beam propagation in an oxide aperture VCSEL structure is not described simply by Gaussian beam propagation theory but mainly by the index guidance due to the oxide aperture. Thus, the extent of beam focusing is considerably smaller than expected by the Gaussian beam propagation theory. A similar reduction of beam focusing was observed for the MEMS-tunable VCSEL with a curved DBR mirror (see Fig. 5 of [15]). In conclusion, the focused feedback effect does not account for the mode selection properties of microlens VCSELs.
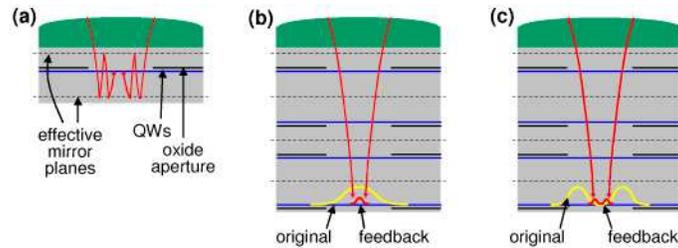

Fig. 4. (a) Schematic illustration of the focused feedback model. Unfolded beam propagation paths of (b) the fundamental mode and (c) a higher order mode.
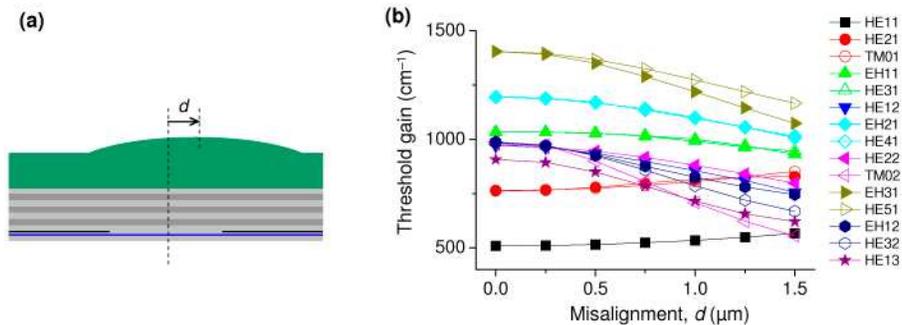

Fig. 5. (b) Threshold gains of 15 modes vs. misaligned distance, d, defined with respect to the center of the oxide aperture, as shown in (a).

In a second set of simulations we investigate the effect of misalignment of the microlens with respect to the oxide aperture on the mode selection properties. Figure 5 shows the calculated threshold gains of the 15 modes in dependence of the misalignment, d. The lens thickness h is set to $46.2\lambda/4$. As shown in Fig. 5(b), the threshold gain of the fundamental mode HE_{11} slowly increases as the misalignment is increased from 0 to 1.5 µm, while the threshold gains of several higher order modes, including TM_{02}, decrease quickly. As a result, the gain difference between the fundamental mode and the next higher order mode, which represents the strength of single mode selection, gets smaller for larger misalignments, and finally the laser turns multi-mode, as the crossing of the modes HE_{11} and TM_{02} near $d=1.5$ µm indicates. The origin of this misalignment dependence can be understood by analyzing the Poynting vector profiles. For $d=0$ µm the fundamental mode, HE_{11}, has low emission loss, as shown in Fig. 6(a1), while the mode TM_{02} has a considerable emission loss originating from the '−' regions that are indicated by the red arrows in Fig. 6(a2). This contrast of emission loss leads to the dominance of the fundamental mode HE_{11} with respect to TM_{02} at $d=0$ µm in Fig. 5(b). For $d=1.5$ µm, the left '−' region that is shifted to the right overlaps to a greater extent with the central mode, as indicated by the red arrow in Fig. 6(b1). This results in an increased emission loss and the slow increase of HE_{11} threshold gain at $d=1.5$ µm in Fig. 5(b). However, with the same misalignment, the mode TM_{02} undergoes a considerable reduction of emission loss in regions indicated by blue arrows in Fig. 6(b2), which explains the fast decrease of TM_{02} threshold gain in Fig. 5(b). As illustrated with the Poynting vector analysis, the misalignment effect on the mode selection results from the alternating distribution of multiple '+' and '−' regions. The computed far-field profile of the fundamental mode at $d=1$ µm, shown in Fig. 6(c), has a small side lobe. This is similar to the measured far-field profile of the first single-mode microlens VCSEL, shown in Fig. 2 of [2]. This indicates that the device had a misalignment of the microlens which, as a drawback, led to a small single mode output power due to the reduced single mode selection strength, as shown in Fig. 5(b).
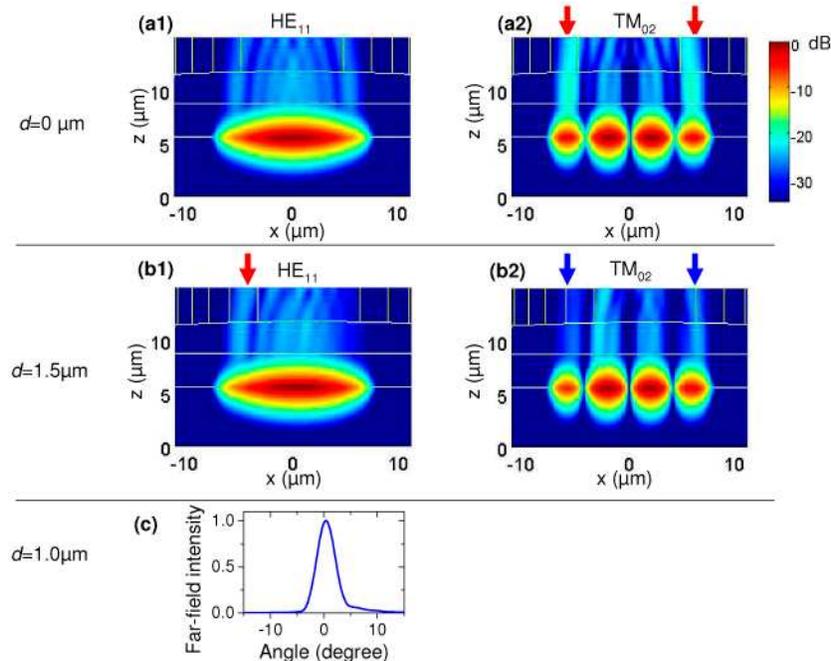

Fig. 6. (a1, a2, b1, b2) Upward Poynting vector profiles. Two modes (HE_{11} and TM_{02}) when the misalignment d = 0 and 1.5 µm, are compared. (c) Far-field profile of d=1 µm case.

This analysis immediately suggests two strategies for avoiding the misalignment problem of reduced single mode selection strength from the microlens VCSEL: (1) to devise a self-

aligned microlens fabrication technique or (2) to invent a microlens configuration which displays a single ' + ' and '−' region. In the next section it is shown that the second approach not only removes the misalignment effect but also provides single mode selection strength comparable to surface relief VCSELs.

4. Thin microlens VCSELs

The new design for single-mode Gaussian emission employs a thin ($\lambda/4$-thick) microlens and a doubled ($2\lambda/4$-thick) topmost DBR layer, as shown in Fig. 1(b). As illustrated in Fig. 7(a), this thin microlens configuration results in a single region of constructive interference, '+' region, in the centre and a single '−' region elsewhere: The doubled topmost DBR layer results in destructive interference outside the microlens region. In this way, the misalignment effect due to the multiple '+' and '−' regions can be avoided. The threshold gain vs. misalignment graph in Fig. 7(b) shows that the threshold gain of HE_{11} is significantly smaller than that of the other modes even up to d=1.5 µm, opposite to the thick lens case in Fig. 5(b). In fact, as the lens is misaligned there is no reduction of emission loss at the region indicated by a blue arrow in Fig. 8(b2). This is opposite to the case in Fig. 6(b2). Considering that a typical lithographic misalignment is ~1 µm, stable single mode operation can be obtained using the thin lens approach.

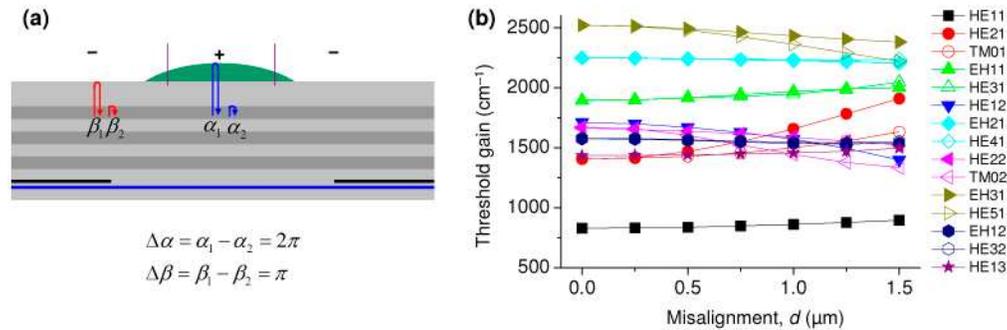Fig. 7. (a) Illustration of phase relations that give rise to the single central region ('+') of constructive interference. The phases α_1, α_2, β_1, and β_2 denotes phase shifts after a round trip or a mere reflection indicated by blue and red arrows. (b) Threshold gains of 15 modes vs. misaligned distance, d.
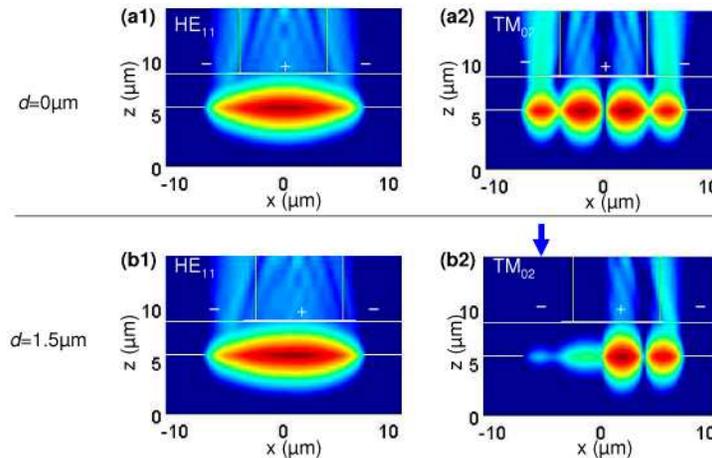

Fig. 8. (a1, a2, b1, b2) Upward Poynting vector profiles. Two modes (HE_{11} and TM_{02}) are compared for different degrees of misalignment, i.e., $d = 0$ and 1.5 µm.

The single mode strength of the thin lens approach was compared to a surface relief VCSEL (reference single mode device), a polymer-microlens surface-relief VCSEL suggested in [9] (reference optical tweezers device with Gaussian emission), and a plain VCSEL (reference multimode device): The device profiles are shown in Fig. 1. The oxide aperture diameter of the thin lens, the surface relief and the plain VCSEL was varied from 6 to 15 µm, while that of the polymer-microlens surface-relief VCSEL was fixed at 8 µm as in [9]. The single mode strength is characterized in terms of the mode stability factor S [13], which is a commonly used parameter in optical simulations of VCSELs:

$$S = (g_1 - g_0)/g_0 \times 100(\%),\qquad(1)$$

Here, g_0 and g_1 are the threshold gains of the fundamental mode and the higher order mode with the next smallest threshold gain, respectively.

The simulation results in Fig. 9 show that the thin microlens VCSEL structure has S values comparable to that of surface relief designs. This is because the microlens VCSEL structure as well as the surface relief structure gains their single mode characteristic from the spatial phase matching condition and not from the beam focusing, as discussed in the previous section. Regarding single mode operation, one may interpret the thin microlens VCSEL as the analogue version of the non-inverted surface-relief VCSEL. At a given oxide aperture, the RoC of the microlens, R and the surface relief diameter, d_{SR} shown in Fig. 9, were chosen so as to lead to the largest S value for the thin microlens VCSEL and the surface relief VCSEL, respectively. An S value of ~70% typically corresponds to a SMSR of 30-dB which is sufficient for many applications. It is anticipated that a thin microlens VCSEL with an appropriate oxide aperture size can achieve single-mode output power level similar to that reported for surface relief structures, i.e. about 6 mW [4, 16].
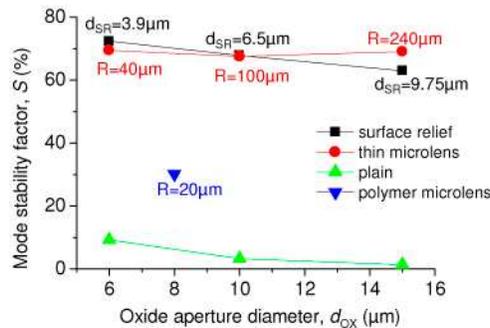

Fig. 9. Mode stability factor, S, vs. oxide aperture diameter, d_{OX}. The radius of curvature, R and the surface relief diameter, d_{SR} of each structure are given.

The relatively small S value of the polymer-microlens surface-relief VCSEL in Fig. 9 explains the poor single mode characteristics that were experimentally observed in [9]. In Fig. 8(b) of [9], the SMSR at the maximum output power (at 16-mA current) is 3–4 dB; thus, the overall emission shape should be a mixture of the fundamental and the first order modes, thereby significantly deviating from the desired Gaussian shape. The thin microlens VCSEL will be able to maintain about 30-dB SMSR even at the maximum output power, similar to surface relief structures. Simultaneous Gaussian-shaped emission (with no broadening of beam width due to mixture with higher order modes) and high differential quantum efficiency due to the single mode operation can thus be obtained. The anticipated high single-mode output power is sufficient for VCSEL-based optical trapping, as discussed in [9].
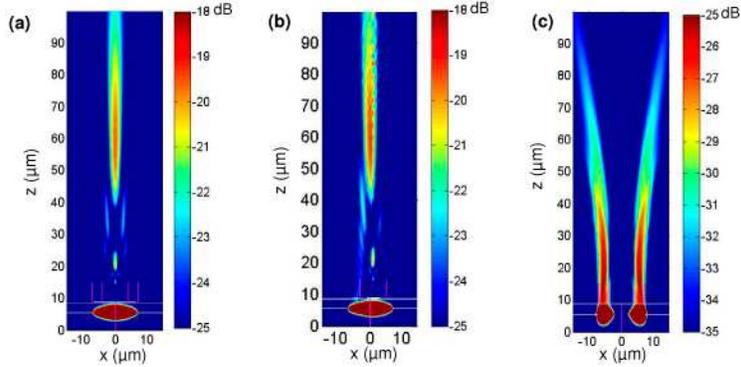
Fig. 10. Beam focusing profiles of (a) d=0 µm case and (b) d=1.0 µm case of the λ/4-thick microlens design for Gaussian-shaped emission. (c) Beam focusing profile of the 2λ/4-thick microlens design for doughnut-shaped emission (d=0 µm). The oxide aperture size is 15 µm for all three cases.

Beam focusing profiles of perfectly aligned and misaligned cases are shown in Fig. 10(a/b). Strong transversal focusing was obtained from the thin microlens structures, regardless of misalignment. This strong transversal focusing will provide sufficient attractive gradient force toward the beam axis, as needed for the optical trapping of high-refractive-index non-absorbing particles. Strong longitudinal focusing is not required, since in VCSEL-based optical trapping, the longitudinal positioning is usually obtained by a cover slip. As shown in Fig. 10(c), a clear doughnut-shaped emission could also be obtained from an alternative structure. This structure employed a thin (2λ/4-thick) microlens and a doubled (2λ/4-thick) topmost DBR layer, as shown in Fig. 1(c). The misalignment influence on threshold gains is relieved in this 2λ/4-thick design as well. An extra objective lens might be necessary in order to further focus the beam. The expected 5–7 mW doughnut-shaped emission at currents lower than 20 mA, makes the thin microlens approach highly advantageous compared to photonic crystal surface emitting lasers, which demonstrated 4 mW output at 95-mA current [11].

We notice that while the investigations of the mode selection properties of thin microlens VCSEL structures in this paper are limited to the short wavelength rage, the basic ideas can of course be applied to improve devices in the long wavelengths.

5. Conclusions

Based on extensive vectorial simulations of VCSELs with surface structuring it has been shown that mode selection properties are strongly affected by spatial filtering in combination with interference effects. In particular, it was suggested that the spatial filtering effect can be used to design microlens VCSEL structures that emit in single-mode Gaussian-shaped or doughnut-shaped emissions. Furthermore, the strength of this mode selection is sensitively influenced by the misalignment of the microlens with respect to the oxide aperture. A novel thin microlens VCSEL structure not only removes the misalignment effect but also provides strong single mode operation comparable to state-of-the-art surface relief VCSELs. This capability of mode shape engineering and beam focusing simultaneously with the achievement of high single-mode output power is highly desirable for many applications such as low cost laser sources for mid-range optical interconnects and compact optical trapping applications.

Acknowledgement